

# Non-hotspot formation of volcanic chains: control of tectonic and flexural stresses on magma transport

Christoph F. Hieronymus<sup>a,\*</sup>, David Bercovici<sup>b</sup>

<sup>a</sup> *Danish Lithosphere Centre, Copenhagen, Denmark*

<sup>b</sup> *Department of Geology and Geophysics, University of Hawaii, Hawaii, USA*

Received 16 March 2000; received in revised form 13 July 2000; accepted 13 July 2000

## Abstract

The South Pacific, in the vicinity of both the superswell and the East Pacific Rise, is replete with volcanic chains that, unlike the Emperor-Hawaiian Chain, defy the hypothesis of formation via the relative motion of plates and hotspots. We propose two nearly identical models for the origin of near-axis and superswell chains, assuming that both regions are underlain by significant quantities of more or less uniformly distributed partial melt. Given an initial volcanic load or a local anomaly in the melt source region, volcanic chains form by magmatic hydrofracture at local tensile maxima of flexural and membrane stresses. Fracture wall erosion by magma flow provides a feedback which results in discrete edifices within the chains. The model predicts island chains aligned with a deviatorically tensile tectonic stress. Near the ridge, the elastic lithosphere is thin, and observations and theoretical considerations indicate a strong deviatorically tensile stress field perpendicular to the ridge axis. Under such conditions, the model results in parallel lines of volcanoes perpendicular to the spreading ridge. Later, interstitial volcanism within the individual chains reduces the average spacing and results in nearly continuous ridges. On the thicker lithosphere of the superswell, membrane stresses are negligible and the model produces chains of much more widely spaced volcanoes. A more isotropic stress field may result in broader chain-like patterns of volcanoes. In both cases, the chains represent self-propagating disturbances; the resulting age progressions are thus independent of plate velocity, but depend only on the dynamics of volcano formation and evolution. © 2000 Elsevier Science B.V. All rights reserved.

*Keywords:* magma transport; volcanism; intraplate processes; hot spots; lithosphere

## 1. Introduction

The South Pacific Superswell is defined as the region surrounding French Polynesia and is about 250–750 m shallower than ‘normal’ sea-floor based on empirical depth–age relations [1–3].

The superswell overlies upper mantle with anomalously slow surface waves [4] and displays a high concentration of volcanic islands [2]. Both the superswell and its eastward extension towards the East Pacific Rise (EPR) (Figs. 1 and 2) are characterized by abundances of seamounts three times higher than on equivalent North Pacific lithosphere [5]. The origin of the seamounts as well as the ‘hotspot’ island chains has been the subject of much debate recently. While island chains elsewhere – such as Hawaii – are well ex-

\* Corresponding author. Tel.: +1-979-845-1309;  
Fax: +1-979-845-6162; E-mail: chris@seaver.tamu.edu

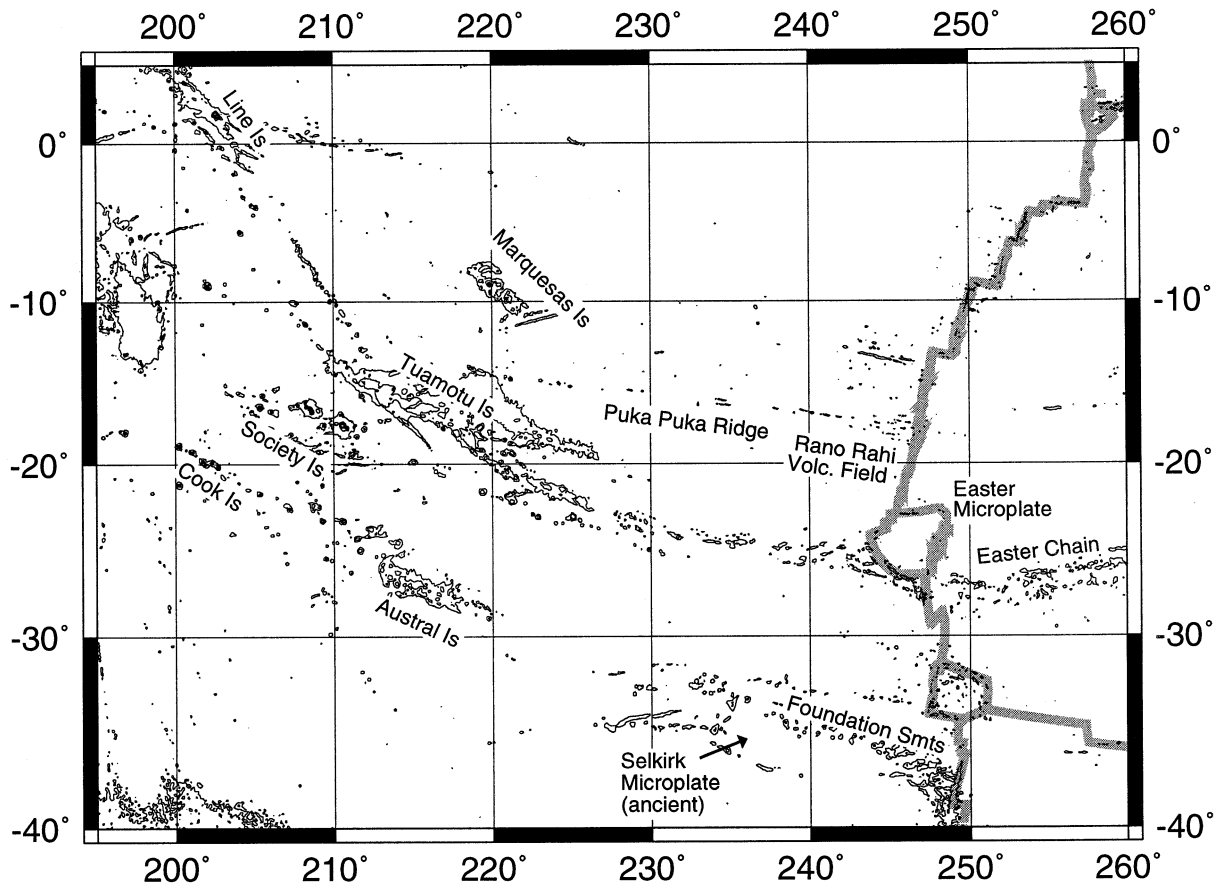


Fig. 1. Map of South Pacific Superswell and southern EPR. Contours are residual bathymetry after subtracting tenth order polynomial trend to show islands and seamounts while neglecting the elevation due to the spreading ridge and other large scale features. Contours are at an arbitrary reference depth and at 2000 m above that depth. Data from [52].

plained by the steady motion of lithospheric plates over stationary hotspots or plumes [6,7], on the superswell even the major island chains do not appear to fit this model [2]. The alignment of the island chains typically deviates from the inferred motion of the Pacific plate [2,8], and the radiometrically determined age progressions are inconsistent with the Pacific plate velocity. The age progressions are in some instances too slow, in others too fast, in the opposite direction, decreasing in age outward in both directions from a central volcano, or they display discrete periods of superimposed volcanism [2].

Smaller seamounts are also typically aligned in chains [9] with the individual cone-shaped volca-

noes often coalescing to form continuous ridges [9,10]. Their formation may be enhanced in, or even limited to, the near-spreading ridge environment [5]. Radiometric ages of the Puka Puka ridge [11] do not support a plume or 'mini-plume' origin [12–14] of the near-spreading ridge seamount chains. For these seamounts, seismic reflectivity indicates recent volcanism from about 30 km to at least 400–500 km away from the EPR [10].

Alternative explanations for the formation of seamount and island chains focus on observations of gravity lineations of various wavelengths; there is some evidence that volcanic activity correlates with such lineations. Seamount activity appears

enhanced in the troughs of small wavelength ( $\approx 150$  km) lineations [11], although this correlation is not perfect and some chains cross from troughs onto crests [11], while in other places, volcanic activity in an active field covers several troughs and crests [10]. The Polynesian island chains instead typically fall on the crests of medium wavelength ( $\approx 1000$  km) gravity lineations [15–17]. If the gravity lineations are the surface expression of convection rolls aligned with absolute plate motion [18,19], then the Polynesian island chains may be explained in terms of ‘hot-

lines’ of convective upwelling [15–17]. The same mechanism has been postulated for the formation of the near-axis seamounts [14,20]. Lithospheric stretching or boudinage due to ridge-parallel tensile stress and subsequent volcanism on the thinned portions of the lithosphere also produce a correlation between gravity lineations and seamount chains (but of opposite sign) [11,21], but there is no evidence of significant extension of the Pacific plate [11,22].

Another type of model explains the origin of near-axis seamounts by preferential, early melting

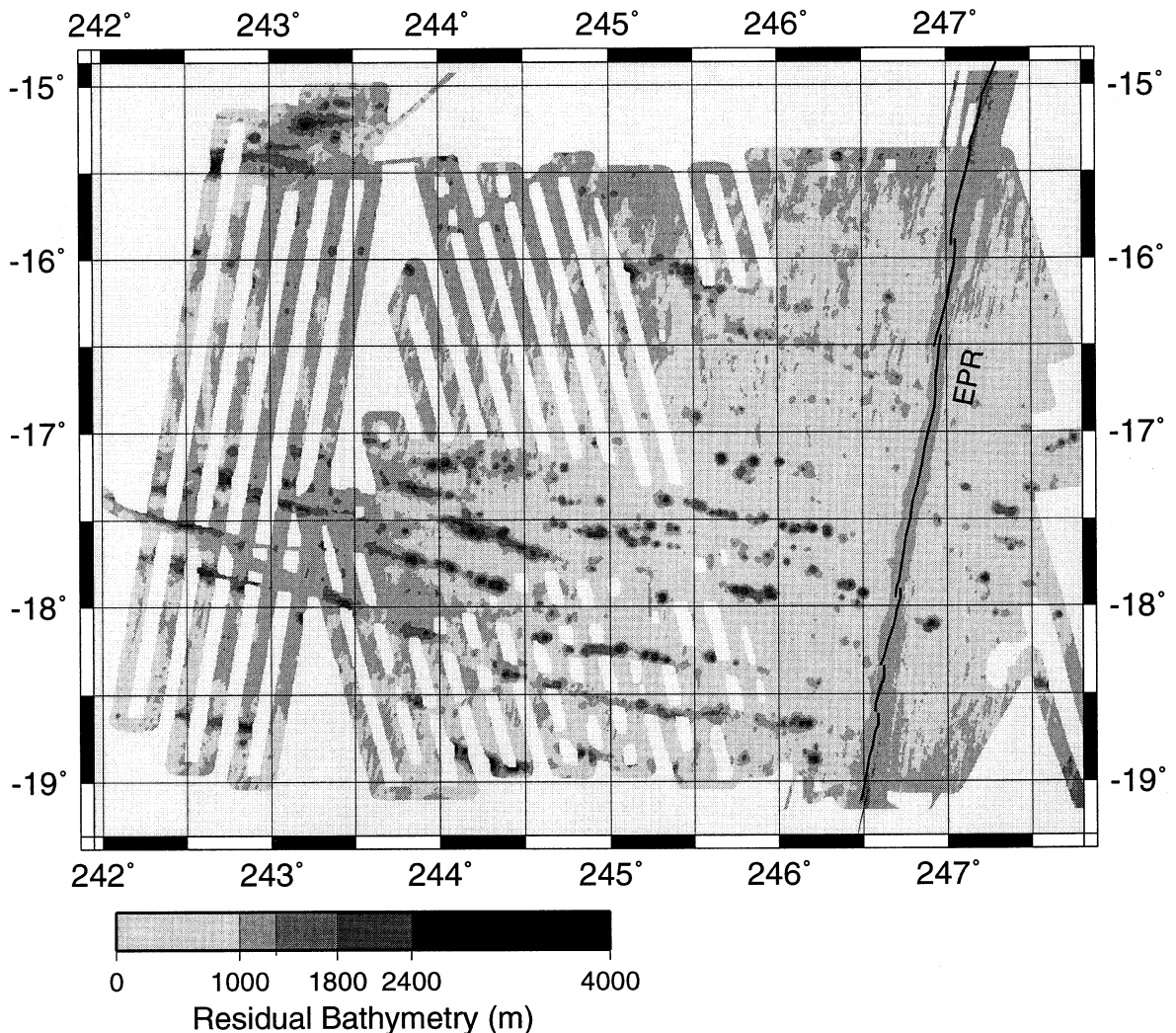


Fig. 2. Map of Rano Rahi volcanic field. Shading shows bathymetry with trend removed as in Fig. 1. Data from [9].

of fertile mantle heterogeneities in the upwelling zone beneath a passive spreading center [23,24]. Such heterogeneities would need to be very elongated or clustered approximately along mantle flow-lines to produce chains 60 km or more in length [10]. Additionally, while small-scale heterogeneities are believed to exist in the mantle [25,26], they are unlikely to be the cause of volcanism far from the ridge since, in that region, mantle flow due to passive spreading does not have a significant vertical component [10].

The model introduced in this paper explains the distribution of non-hotspot island and seamount chains in terms of the vulnerability of the lithosphere to magma penetration due to lithospheric stresses and the effects of melting of the conduit walls [27]. The availability of melt is assumed to be controlled by large scale mantle processes such as convection under the superswell [28] or return mantle flow toward the EPR from the superswell bringing in anomalously hot asthenosphere material [28,29], resulting in an abundant melt supply throughout much of the superswell region and near the EPR. Volcanism is activated or suppressed by tensile and compressive stresses, respectively, which are made up of a combination of tectonic and flexural stresses. Strong evidence for tectonic stress control on alignment of seamount chains comes from the EPR at 5°N to 15°N, where absolute and relative plate motion differ significantly. In this region, two distinct groups of seamount chains are found, one in which the chains are aligned with absolute plate motion, and another one with the chains paralleling the relative plate motion of the Pacific and the Cocos plate [30]. While the chains aligned with absolute motion indicate an origin due to a stationary melting anomaly in the mantle, it is difficult to envision a mechanism for the formation of the chains parallel to relative plate motion that does not incorporate the tectonic stress field.

The state of stress in the lithosphere of a vast part of the world's oceans remains unknown due to both a scarcity of observations [31] and an incomplete understanding of the plate tectonic driving forces [32,33]. The most important observational constraint is that the tectonic stress field is mostly compressive throughout, but with a nar-

row region subject to normal faulting near the spreading ridges [31]. While simple force balances indicate that a compressive stress field may be produced by a dominant balance of ridge-push force versus friction at the trench [32,34], the state of stress parallel to the spreading ridge is even more poorly understood; in the south eastern Pacific, the plate is bounded mostly by transform faults to the south, and a retreating trench to the north [35]. While Sandwell et al. [11] argue for a net tensile stress perpendicular to the ridge axis of the EPR, (resulting in boudinage and formation of volcanic chains on the thinned parts of the lithosphere), we propose an alternative origin of the volcanic chains which predicts a deviatoric tensile stress in the direction of relative plate motion.

## 2. Theory

Transport of magma through the brittle part of the lithosphere is assumed to occur via fractures. As the purpose of the model is not to predict the orientation or evolution of individual dikes, but only their time- and space-integrated ability to transport magma, we assume that dikes form as soon as the local magma pressure is greater than the sum of the tensile strength of the lithosphere and the least compressive horizontal stress in the lithosphere. The effect of the dikes on magma transport is modeled by the permeability of the lithosphere, which depends on the magma pressure and the local stress field, as well as erosion of the conduit walls [27].

Melt is assumed to be distributed uniformly at the base of the lithosphere. While this assumption may not hold perfectly either on the superswell or near the EPR, it does show most clearly what type of filter the lithosphere provides in determining the location of volcanism with regard to the melting anomalies within the mantle.

The stress field is composed of a regional tectonic stress field, flexural stresses, and – on thin lithosphere – membrane stresses. The total flexure (including flexural and membrane stresses, but neglecting tectonic stresses) is described by two coupled, non-linear differential equations [36,37]

$$\nabla^4 F = E \left[ \left( \frac{\partial^2 w}{\partial x \partial y} \right)^2 - \frac{\partial^2 w}{\partial x^2} \frac{\partial^2 w}{\partial y^2} \right] \quad (1)$$

$$\nabla^4 w = \frac{12(1-\nu^2)}{EH^2} \left( \frac{(\rho_m - \rho_w)gh}{H} + \frac{\partial^2 F}{\partial y^2} \frac{\partial^2 w}{\partial x^2} + \right. \\ \left. \frac{\partial^2 F}{\partial x^2} \frac{\partial^2 w}{\partial y^2} - 2 \frac{\partial^2 F}{\partial x \partial y} \frac{\partial^2 w}{\partial x \partial y} - \Delta \rho g w \right) \quad (2)$$

where  $x$  and  $y$  are the horizontal coordinates,  $w$  is the vertical deflection of the lithospheric plate,  $F$  is a stress function,  $\rho_m$ ,  $\rho_l$ ,  $\rho_a$ , and  $\rho_w$  are the densities of the magma, the lithosphere, the asthenosphere, and of water, respectively,  $h(x,y)$  is the height of the surface load of density  $\rho_m$ ,  $E$  is Young's modulus,  $H$  is the effective elastic thickness of the lithosphere,  $\nu$  is Poisson's ratio, and  $\nabla^4 = (\partial^4/\partial x^4 + 2\partial^4/\partial x^2\partial y^2 + \partial^4/\partial y^4)$  is the horizontal biharmonic operator. The density difference  $\Delta\rho = (\rho_a < \rho_m)$  in the last term of Eq. 2 assumes that the moat is largely filled with volcanic debris [38] of the same density as the volcanic edifice. With  $F=0$  in Eq. 2, the familiar thin-plate flexural equation is recovered; the stress function  $F$ , defined by Eq. 1, and the additional terms in Eq. 2 are derived by considering the force balance due to large deflections on a small element located on the mid-level plane of the plate, which is stress free in thin plate theory [36].

On old, thick lithosphere, even large volcanoes such as Mauna Loa in Hawaii cause only small deflections of the lithosphere on the order of 3–5 km [39] compared with the elastic thickness of the plate, which is about 30 km [39]. The thin-plate approximation is therefore valid (membrane stresses are negligible) and the deflection is described by Eq. 2 with  $F=0$ , yielding a single, linear flexural equation [36]. For young lithosphere, the plate thickness may be as low as 500 m or less [38] with deflections of the same order, and thus the membrane stresses have to be taken into account. Horizontal stresses (such as a tectonic stress) potentially affect the flexural displacement as well [37]; however, it can be shown that, for the stresses (tens of MPa) and plate thicknesses ( $\geq 500$  m) considered here, their effect is negligible and hence use of Eqs. 1 and 2 is appropriate.

Only the stresses near the surface will be considered as this is where fracturing is most likely to occur [40]. At depth, a transport mechanism different from flow through brittle fractures is likely to be operating. Evidence of this is seen in volcanism near the flexural bulges north and south of Hawaii [41] where the flexural stresses at depth are compressive.

The flexural stresses associated with plate deformation are given by

$$\sigma_{xx}^{\text{flex}} = -\frac{EH}{2(1-\nu)} \left( \frac{\partial^2 w}{\partial x^2} + \nu \frac{\partial^2 w}{\partial y^2} \right) \quad (3)$$

$$\sigma_{yy}^{\text{flex}} = -\frac{EH}{2(1-\nu)} \left( \frac{\partial^2 w}{\partial y^2} + \nu \frac{\partial^2 w}{\partial x^2} \right) \quad (4)$$

$$\sigma_{xy}^{\text{flex}} = -\frac{EH}{1+\nu} \frac{\partial^2 w}{\partial x \partial y} \quad (5)$$

and the membrane stresses are

$$\sigma_{xx}^{\text{mem}} = \frac{\partial^2 F}{\partial y^2} \quad (6)$$

$$\sigma_{yy}^{\text{mem}} = \frac{\partial^2 F}{\partial x^2} \quad (7)$$

$$\sigma_{xy}^{\text{mem}} = \frac{\partial^2 F}{\partial x \partial y} \quad (8)$$

The normal and shear components of these stresses are added to the corresponding components of the regional stress field to yield the three total stress components  $\sigma_{xx}$ ,  $\sigma_{yy}$ , and  $\sigma_{xy}$  as functions of  $x$  and  $y$ . The local maximum eigenvalue of the total two-dimensional stress tensor, representing the most tensile principal stress, may be found using [37]

$$\sigma_{\text{max}} = \frac{1}{2}(\sigma_{xx} + \sigma_{yy}) + \left[ \frac{1}{4}(\sigma_{xx} - \sigma_{yy})^2 + \sigma_{xy}^2 \right]^{1/2} \quad (9)$$

Following Hieronymus and Bercovici [27,42], we formulate the complete dynamical model by defining the permeability of the lithosphere which

in turn controls the melt transport via a Darcy flow law. We assume that the porosity  $f$  of the lithosphere due to magma-filled cracks and fractures is controlled by the stress field and erosion of the fracture walls [27,42]

$$Cdf = Bd\varepsilon + d\sigma_{\max} + d\sigma_m \quad (10)$$

where  $d\varepsilon(x,y)$  is the net energy input per volume of the bulk medium consisting of magma and wall rock. Energy inputs which induce erosion include heat (for melting and thermal conditioning), gravitational potential energy, internal mechanical energy, kinetic energy (for mechanical and thermo-mechanical erosion), and chemical potential energy (for reactive and hydrating effects). The non-lithostatic melt pressure at the base of the lithosphere is given by  $\sigma_m$ ,  $B$  is a constant, and  $C$  is a parameter whose inverse  $C^{-1}$  represents the responsiveness of crack or dike volume to stress and erosion. We assume that parameter  $C$  is a function of  $f$ ; a simple relation ( $C = C_0 / (f(f_{\max} - f))$ ) captures the essential physics by precluding meaningless values of  $f < 0$  and  $f > f_{\max}$ . The parameter  $f_{\max}$  is a maximum porosity beyond which increases in stress or total energy are partitioned less into changing porosity than into other responses, such as heating or deforming the magma. The numerical value of  $f_{\max}$  need not be specified as  $f_{\max}$  only appears in products with other parameters.

Eq. 10 may be integrated using the above relation for  $C$ . Assuming a linear dependence of permeability on porosity, it follows that

$$k = \frac{k_0 f_{\max}}{2} \left[ 1 + \tanh \left( \frac{\sigma_{\max} + \sigma_m - \sigma_o + B\varepsilon}{2C_0 / f_{\max}} \right) \right] \quad (11)$$

where  $k_0$  is a reference permeability and  $\sigma_o$  is an integration constant representing the tensile strength of the lithosphere.

The Darcy flow law governing melt transport through fractures (assuming laminar flow) is

$$V = \frac{k}{\mu} \left[ (\rho_l - \rho_m)g - ((\rho_m - \rho_w)h + \rho_a w) \frac{g}{H} \right] \quad (12)$$

where  $\mu$  is the dynamic magma viscosity. Magma is assumed to solidify in place as it reaches the surface; outwardly horizontal spreading of the volcanic edifice due to gravity is neglected. The growth of the volcano is then described by

$$\frac{\partial h}{\partial t} = V \quad (13)$$

The net energy content  $\varepsilon$  per volume of the bulk medium changes primarily due to injection of magmatic net energy, which is proportional to  $V$ :

$$\frac{\partial \varepsilon}{\partial t} = \frac{\Delta Q}{H} V \quad (14)$$

where  $Q$  is the drop in magmatic energy per volume across the lithosphere (from bottom to top). The energy variable  $\varepsilon$  may be eliminated from the problem by noting from Eqs. 13 and 14 that  $\varepsilon$  is proportional to  $h$  up to a constant. Setting  $\varepsilon(t=0) = h(t=0) = 0$ , we can thus write  $\varepsilon = \Delta Q h/H$ .

Eqs. 1–13 and the above relation for  $\varepsilon$  form a complete set when combined with the boundary conditions that  $h$ ,  $w$ ,  $V$ , and all stresses except for the tectonic stress vanish far from the region of interest; initial conditions will be specified in the next section. The equations may be non-dimensionalized using the length, time, and pressure scales  $\hat{X} = [EH^3/(12(1-\nu^2)g\Delta\rho)]^{1/4}$ ,  $\hat{T} = H\mu/[gk_0(\rho_l - \rho_m)]$ , and  $\hat{P} = \rho_l g H$ , respectively. The length scale is proportional to the flexural parameter, while the pressure scale is equal to the lithospheric overburden. The time scale is the time required for traversal of the lithosphere at the Darcy velocity with maximum permeability and with a driving pressure equal to the lithospheric overburden. After non-dimensionalization and some simplification, the equations are

$$\nabla^4 F = a_1 \left[ \left( \frac{\partial^2 w}{\partial x \partial y} \right)^2 - \frac{\partial^2 w}{\partial x^2} \frac{\partial^2 w}{\partial y^2} \right] \quad (15)$$

$$\nabla^4 w = a_2 h - w +$$

$$a_3 \left( \frac{\partial^2 F}{\partial y^2} \frac{\partial^2 w}{\partial x^2} + \frac{\partial^2 F}{\partial x^2} \frac{\partial^2 w}{\partial y^2} - 2 \frac{\partial^2 F}{\partial x \partial y} \frac{\partial^2 w}{\partial x \partial y} \right) \quad (16)$$

Table 1  
Non-dimensional parameters

Parameter	Description
$a_1$	$\frac{E}{\rho_l g H}$
$a_2$	$\frac{\rho_m - \rho_w}{\Delta \rho}$
$a_3$	$\frac{\rho_l}{\Delta \rho} \left( \frac{12 H g \Delta \rho (1 - \nu^2)}{E} \right)^{1/2}$
$a_4$	$\frac{1}{2(1 - \nu) \rho_l} \left( \frac{12 E^3 \Delta \rho (1 - \nu^2)}{H^3 g^3} \right)^{1/4}$
$a_5$	$\frac{1}{(1 - \nu) \rho_l} \left( \frac{12 E^3 \Delta \rho (1 - \nu^2)}{H^3 g^3} \right)^{1/4}$
$a_6$	$\frac{\rho_l g H f_{\max}}{C_o}$
$a_7$	$\frac{B \Delta Q f_{\max}}{C_o} \left( \frac{E}{12 g H \Delta \rho (1 - \nu^2)} \right)^{1/4}$
$a_8$	$\left( \frac{12 g H \Delta \rho (1 - \nu^2)}{E} \right)^{1/4}$
$a_9$	$\frac{\rho_m - \rho_w}{\rho_l - \rho_m}$
$a_{10}$	$\frac{\rho_a}{\rho_l - \rho_m}$

$$\frac{\partial h}{\partial t} = \frac{1}{2} \left[ 1 + \tanh(a_6(\sigma_{\max} - \sigma_o) + a_7 h) \right] \times (a_8 - a_9 h + a_{10} w) \quad (17)$$

where  $\sigma_{\max}$  is given by (Eq. 9) and

$$\sigma_{xx} - a_4 \left( \frac{\partial^2 w}{\partial x^2} + \nu \frac{\partial^2 w}{\partial y^2} \right) + \frac{\partial^2 F}{\partial y^2} + \sigma_{xx}^{\text{tec}} \quad (18)$$

$$\sigma_{yy} - a_4 \left( \frac{\partial^2 w}{\partial y^2} + \nu \frac{\partial^2 w}{\partial x^2} \right) + \frac{\partial^2 F}{\partial x^2} + \sigma_{yy}^{\text{tec}} \quad (19)$$

$$\sigma_{xy} = -a_5 \frac{\partial^2 w}{\partial x \partial y} - \frac{\partial^2 F}{\partial x \partial y} + \sigma_{xy}^{\text{tec}} \quad (20)$$

The non-dimensional parameters  $a_1$  to  $a_{10}$  are explained in Table 1. Aside from a non-linearity in the stress field, equations for the lithospheric plate of finite thickness, the set of equations contains a non-linear feedback in Eq. 17 due to erosion of the conduit walls which causes the formation of discrete volcanic edifices instead of spatially continuous or widely distributed ones [27,42].

### 3. Results

The equations are solved using a pseudo-spectral code [43] with  $128 \times 128$  modes, implicit time stepping for the linear parts of the equations and explicit integration for the non-linear parts. For the finite thickness plate, the flexural equation is iterated over until the solution converges.

The governing equations exhibit perfect translational symmetry in both horizontal directions; thus, an initial perturbation is required in all cases

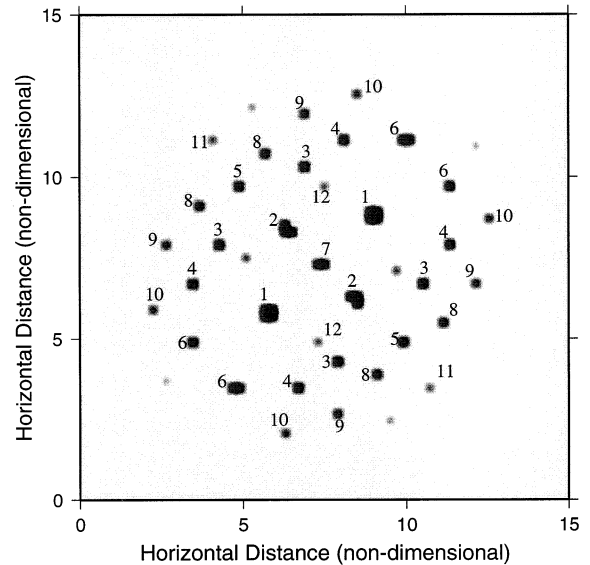


Fig. 3. Map view of pattern of volcanoes resulting from flexural stress and two point loads (labeled 1) as initial perturbations. Subsequent volcanoes form in order indicated by numbers. Non-dimensional parameters used to generate the figure are:  $a_1 = 60.0$ ,  $a_2 = 0.696$ ,  $a_3 = 0.527$ ,  $a_4 = 23.9$ ,  $a_5 = 28.6$ ,  $a_6 = 7.79 \times 10^7$ ,  $a_7 = 3.60 \times 10^7$ ,  $a_8 = 0.597$ ,  $a_9 = 2.00$ ,  $a_{10} = 4.13$ .

to localize the volcanic activity. Fig. 3 the model results for a thick lithospheric plate (for which the thin-plate approximation holds) without tectonic stress. Two volcanic edifices were used as initial disturbance since a single volcano would cause a radially symmetric flexural stress field and thus result in formation of concentric, ring-shaped volcanoes. The results depicted in Fig. 3 indicate an outwardly radiating pattern of volcanoes. The spacing is given by the distance from the volcanic load to the location of maximum tensile stress, which (for a value of  $\nu=0.25$ ) is 0.46 times the distance to the peak of the flexural bulge. Further volcanoes typically form later in the center of any three neighboring volcanoes, thus reducing the average spacing by a factor of about 0.4.

In Fig. 4, output is shown from the same model with a tensile tectonic stress and with a single volcanic edifice as initial perturbation. Here it is the external stress field which breaks the radial symmetry around the point load. A straight line of volcanoes is formed which is aligned with the regional tensile stress direction. The intervolcanic spacing is again determined by the distance from the center of the volcanic load to the position of maximum tensile stress. Dimensionalizing with  $H=5$  km,  $E=7.0 \times 10^{10}$  Pa-s and  $\Delta\rho=700$

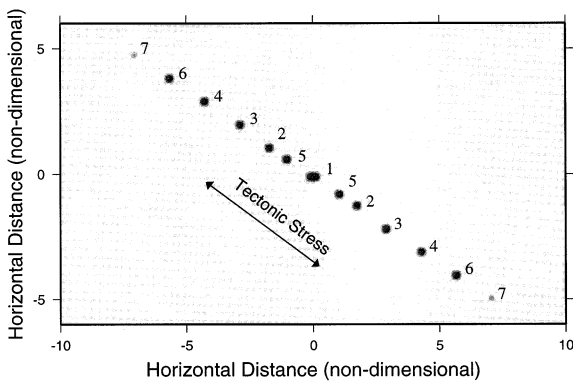


Fig. 4. Line of volcanoes resulting from interaction of flexural stresses and tensile tectonic stress (in direction of volcanic line). Volcanoes indicated by arrows formed as second stage of eruptions after formation of the original line. Non-dimensional parameters used are:  $a_1=420$ ,  $a_2=0.696$ ,  $a_3=0.199$ ,  $a_4=103$ ,  $a_5=123$ ,  $a_6=5.15 \times 10^5$ ,  $a_7=7.00 \times 10^6$ ,  $a_8=0.367$ ,  $a_9=2.00$ ,  $a_{10}=4.13$ . The non-dimensionalized tectonic stresses are:  $\sigma_{xx}^{ec}=0.082$ ,  $\sigma_{yy}^{ec}=0.038$ ,  $\sigma_{xy}^{ec}=-0.057$ .

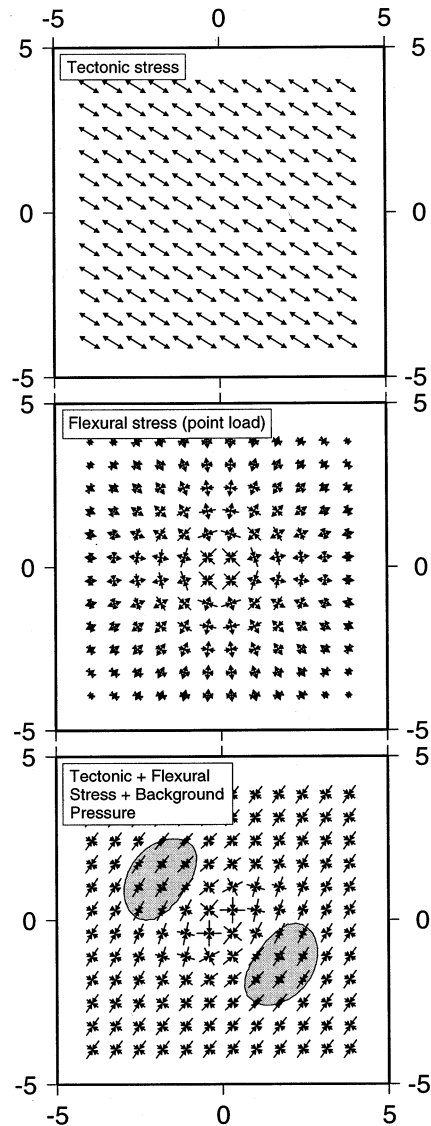


Fig. 5. Map view of principal stresses due to tectonic stress of non-dimensional magnitude 0.31 (upper panel), flexural stress caused by a point load of non-dimensional weight 0.23 (middle panel), and a combination of both (lower panel). The arrows were scaled such that length = (magnitude)<sup>1/4</sup> in order to show weak stresses more clearly. A constant background pressure of magnitude 0.51 was added (lower panel) representing either a compressive non-deviatoric part of the tectonic stress or the tensile lithospheric strength. The pressure keeps the unperturbed lithosphere impermeable. Shaded regions indicate locations where maximum principal stress is tensile.

$\text{kg/m}^3$ , the volcanic spacing is about 25 km. With  $\mu = 100 \text{ Pa}\cdot\text{s}$ ,  $\rho_l = 3400 \text{ kg/m}^3$ ,  $\rho_m = 2600 \text{ kg/m}^3$ , and  $k_o = 3.7 \times 10^{-11} \text{ m}^2$ , the time scale of volcano formation until the edifice reaches 95% of its final height is 1.0 Ma. The propagation velocity of the chain is then 5.4 cm/yr, yielding an average age difference of 460 kyr between adjacent volcanoes. The relative time scales of volcano formation and chain propagation depend on the non-dimensional parameters; the absolute value of the time scales is given by the dimensionalization scale  $\hat{T}$ .

Fig. 5 demonstrates how the interaction of tectonic stresses and flexural stresses due to a point load results in localized tensile stress maxima in the lithosphere where the next volcanoes form. The volcanic ages become increasingly younger outward from the initial, central volcano. The propagation velocity of volcanic activity depends on the rate with which the individual edifices form as well as on the size of load sufficient to initiate the next volcano, which is a function of the rela-

tive magnitudes of  $\sigma_o$ ,  $\sigma_m$ ,  $h$ , and  $\sigma_{\text{tec}}$ . A second, later stage of volcanism results in the formation of further edifices mid-way between the volcanoes of the first set. Further volcano formation was not observed, although it should be noted that the cut-off time for stopping the numerical calculations is somewhat arbitrary; since the lithospheric permeability is small, but non-zero everywhere, then as  $t \rightarrow \infty$ , the model will tend to a single volcanic edifice covering all space with uniform height. As a practical solution, we stopped the computation if no new volcanism was initiated over a time scale which is long in comparison with the time scale of volcano evolution. As any later eruptions begin with very low permeability, magma solidification in the conduit is likely to counteract the effect of the feedback due to conduit wall erosion and preclude the eruption. For simplicity, the details of the thermodynamics including solidification of magma at low flow rates were neglected in the model.

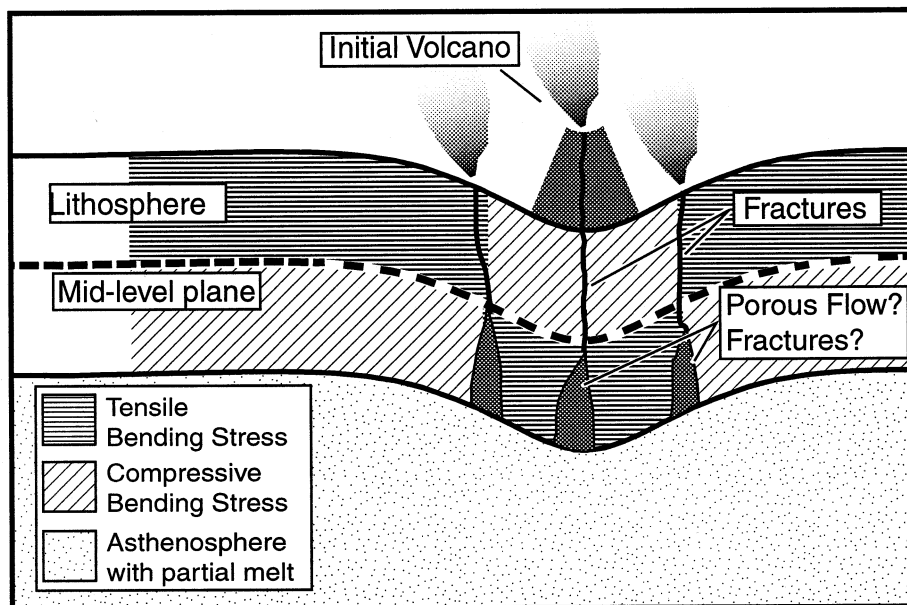


Fig. 6. Sketch of the stresses in the lithosphere due to a volcanic load, also indicating the possible location of the next eruption. The bending stress, whose sign is indicated by shading, varies linearly with depth and is antisymmetric about the mid-plane of the lithosphere. Membrane stresses, which are independent of depth, are caused by local extension or compression of the mid-level plane of the lithosphere, which is indicated by a thick, dashed line; underneath the volcanic edifice, membrane stresses are mostly tensile. The relative magnitudes of bending and membrane stresses are determined by the ratio of the flexural displacement to the plate thickness.

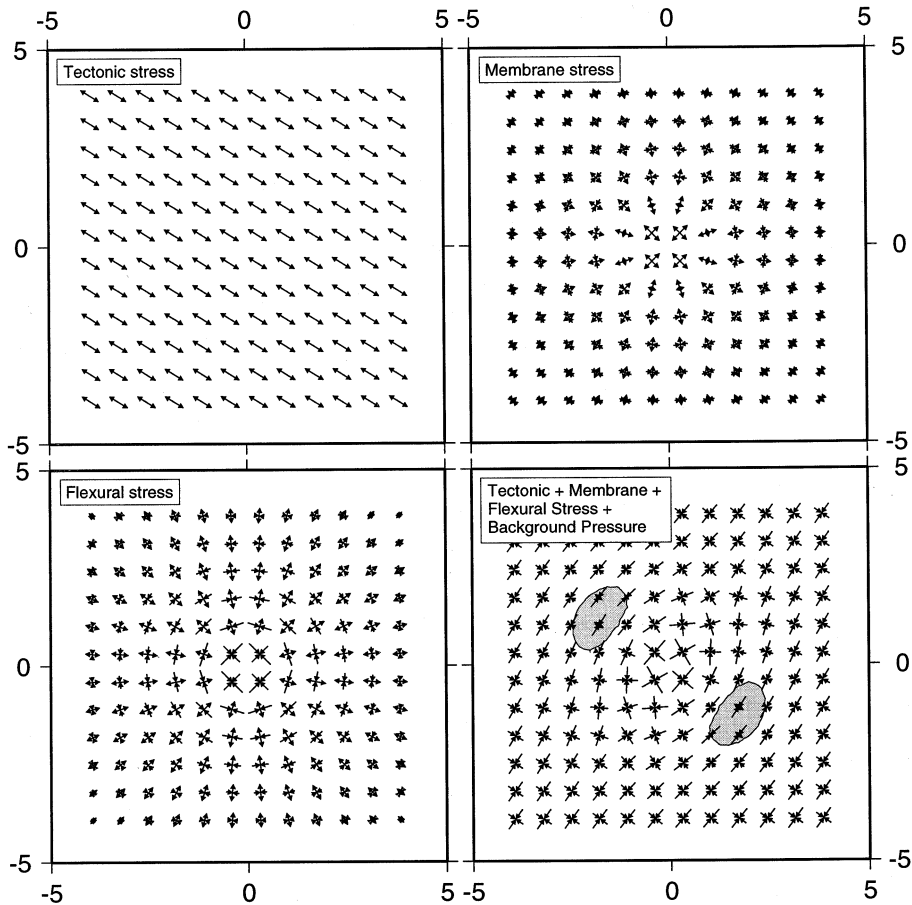


Fig. 7. Principal stresses due to tectonic stress of non-dimensional magnitude 0.23 (upper left panel), membrane stresses caused by point load of weight 0.226 (upper right panel), flexural (bending) stresses (lower left panel) and a combination of all three plus a constant compressive pressure of magnitude 0.52 (lower right panel). Non-dimensional lithospheric thickness is 0.2. Arrows were scaled as in Fig. 5.

The existence of large deflections of the lithosphere in comparison with its thickness requires the use of the flexural equations for a plate of finite thickness, thus introducing membrane stresses into the problem (see Fig. 6). When initialized with a single point-perturbation, the model again produces a line of volcanoes. The volcanic spacing is smaller than that for the equivalent thin-plate approximation because, for the parameters chosen, the mostly tensile membrane stresses are of the same order of magnitude as the bending stresses (see Fig. 7). Close to the volcanic load, the compressive flexural stresses

dominate, but decay with distance more rapidly than the tensile membrane stresses. The location of maximum tensile stress (where the next volcano forms) is thus moved closer to the center of the flexural depression. The degree to which the flexural deflection is governed by either the bending stresses or by the membrane stresses (which is given by the magnitude of the vertical deflection relative to the plate thickness) determines how close to the first edifice the next eruption will start. The possible intervolcanic spacing ranges from the maximum predicted by thin-plate theory (described above) to a minimum of zero spacing

(i.e. a continuous ridge) for a system dominated entirely by the membrane stresses.

Even if bending and membrane stresses are of the same order and there is thus a significant distance between adjacent volcanoes, a series of later eruptions fills in the space between the edifices, eventually creating a nearly continuous ridge. Due to the tensile membrane stresses, several volcanoes typically form in the space between any two volcanoes of the initial chain. This is in contrast with the solution containing only flexural stresses, where over reasonable time spans only one further volcano was observed to form between any two of the older ones.

Membrane stresses perpendicular to the axis of the volcanic line or ridge also interact with the flexural stresses to generate volcanism away from the axis. This off-axis volcanism eventually forms additional lines of volcanoes parallel to the first one. The spacing between the individual lines is of the same order as the spacing between the first edifices within the initial line. Eventually, further lines of volcanoes are formed in parallel, with some in-fill of additional volcanoes in between. Fig. 8 shows model results before the output became excessively convoluted; as mentioned above, slowly developing late stage eruptions are probably suppressed thermodynamically by solidification of magma in the conduit. Dimensionalizing with  $H=2000$  m, volcanoes within each chain are about 5.5 km apart, while the spacing between chains is around 19 km.

#### 4. Discussion

Our model assumes that the lithosphere of the South Pacific superswell and in some near-ridge environments is underlain by large quantities of partial melt. Without perturbations and/or tectonic stresses, the lithosphere forms an impenetrable lid where the tensile strength of the rock and possibly a generally compressive tectonic stress regime preclude the formation of magma fractures. In our model, approximate alignment of volcanic lines with plate motion indicates deviatoric tension in that direction.

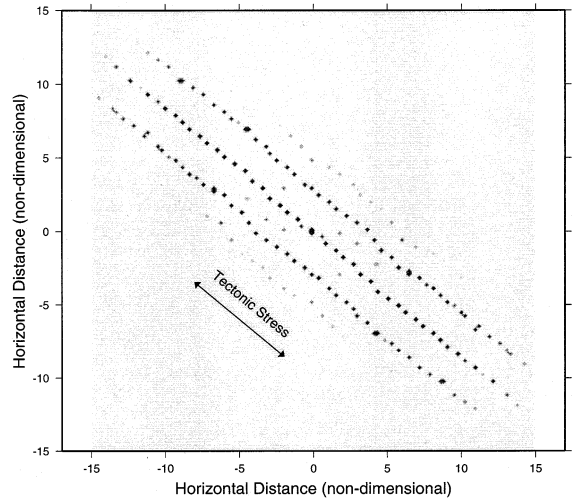


Fig. 8. Multiple lines of volcanoes resulting from interaction of flexural, membrane, and tectonic stresses. Non-dimensional parameters used are:  $a_1 = 2.10 \times 10^3$ ,  $a_2 = 0.300$ ,  $a_3 = 0.135$ ,  $a_4 = 279$ ,  $a_5 = 335$ ,  $a_6 = 175$ ,  $a_7 = 5.00 \times 10^9$ ,  $a_8 = 0.199$ ,  $a_9 = 0.375$ ,  $a_{10} = 4.13$ . The non-dimensionalized tectonic stresses are:  $\sigma_{xx}^{tec} = 0.225$ ,  $\sigma_{yy}^{tec} = 0.675$ ,  $\sigma_{xy}^{tec} = 0.390$ .

#### 4.1. Volcanism on the South Pacific superswell

Volcanism on the relatively old lithosphere of the South Pacific superswell is dominated by and perhaps limited to [5] the large volcanic chains of the Tuamotu Islands, the Society Islands, the Cook and Austral chain, and the Marquesas Islands to the north.

Strong evidence against a mantle plume origin for at least the Cook and Austral chains derives from inconsistent age progressions [2]. The Society Islands extend hundreds of kilometers south-eastward beyond the point of ‘zero age’ [2]; if both parts of the chain are of the same origin, then the plume theory fails also for the Society Islands. The fact that geometric techniques [8] do not clearly locate any fixed hotspots on the superswell may indicate that none of these chains are the product of hotspots.

We thus propose that the chains on the superswell are caused, at least in part, by the stress field. Volcanic chains whose age progressions are impossible to reconcile with plate motion over stationary hotspots are likely to be self-propagat-

ing disturbances of volcanic loads and associated flexure with a more-or-less uniform sublithospheric melt distribution as illustrated in Fig. 4. Other chains are either generated by the same mechanism, or by plumes that are too weak to penetrate the lithosphere on their own; above these plumes, melt migration may be aided by tectonic and flexural stresses, such that the chains are self-propagating, but at the same time limited in extent to the melting region of the plume. The initial perturbation required to start the island chains may be provided by a change in the tectonic stress field due to a plate motion reorganization (which is amplified locally by an inhomogeneity in the lithosphere), the formation of a small sublithospheric melting anomaly, or a change in convection. There is some evidence that mid-plate volcanism or periods of volcanism initiate at times of plate motion changes. On or near the superswell, the start of volcanism in the McDonald chain (within the Austral chain) around 4 Ma [44] may correlate with plate motion changes at 5 Ma [45] or 3 Ma [8]; volcanism in the Cook Islands at 25 Ma [2] correlates with a plate motion change at that time [46,47]; volcanic events in the Line Islands at 89 and 39 Ma (or possibly 43 Ma) [48] correlate with plate motion changes at 84 Ma [49] and 43 Ma [46], respectively; and volcanism in the Foundation chain at  $> 21$  Ma [50] possibly correlates with the 25 Ma plate motion change [46,50]. Once the first volcanic load has been emplaced following some local perturbation, the next volcano forms near the flexural bulge of the first edifice where the surface flexural stresses are most tensile. Such volcanism located on or near flexural arches has been observed both as late stage flood volcanism in Hawaii [41] and as secondary chains in the Austral Islands [44]; it therefore seems plausible that the volcanoes within the chains form on the flexural bulge of the next older volcano, as predicted by the model.

The general alignment of volcanoes suggests that a deviatoric tensile stress field interacts with the flexural stresses to generate local stress maxima which cause the volcanoes to form chains rather than area-covering patterns as demonstrated in Fig. 1. Additional perturbations in form of tectonic fabric or near-axis generated sea-

mounts may cause deviations from perfectly linear chains, resulting in the typically observed wider volcanic patterns within the chains (Fig. 3). Alternatively, the availability of melt may be concentrated along the maxima of the intermediate wavelength ( $\approx 1000$  km) gravity anomalies. In this case, the volcanoes may be mostly radiating outward in a pattern similar to that in Fig. 3, but be constrained to chain-like patterns by a dearth of melt away from the maximum of the gravity lineations. Both models are consistent with the observation that mid-plate stresses are typically not strongly deviatoric [31].

#### 4.2. *Volcanism near the East Pacific Rise*

While the morphology of volcanism near the East Pacific Rise (EPR) is strikingly different from the mid-plate volcanoes of the superswell, we propose that the mechanism generating both types of volcanism is largely identical. The differences are due to a thinner lithosphere and a more coherent stress field near the EPR.

As explained in Section 2, a thin lithosphere with respect to the amplitude of the flexural displacement necessitates the use of the equations for a plate of finite thickness, which results in coalescence of individual volcanoes into a continuous ridge over time. Flexural studies indicate that the lithosphere near the EPR has an elastic thickness of 0–1 km around 500 km from the ridge axis, increasing to 3–4 km at a distance of 2500 km from the axis [38]. While the flexure underneath the volcanic loads has not been observed directly, volcanic heights on the order of 200–2000 m and diameters of several kilometers [9,10] suggest that the resulting deflection must be significant in comparison with the lithospheric thickness. The predicted coalescence of volcanoes is clearly observed in the Rano Rahi volcanic area [9,10]. Signs of active or recent volcanism are existent from the near-ridge environment out to at least 500 km from the ridge axis [10]. It thus seems reasonable to interpret the distance from the ridge as a snapshot of a steady-state temporal evolution of volcanism. Volcanic activity commences some 30 km from the EPR in form of small, individual cones [10]. The cones increase

in height away from the ridge. A transition from distinct to overlapping volcanoes occurs at a distance of 75–200 km from the ridge axis, while a further change to continuous ridges occurs at a distance of about 500 km [10]. The predictions of the model of volcanic lines formed initially with fairly large intervolcanic spacing and a subsequent decrease in spacing by additional eruptions within the individual lines is thus in excellent agreement with the observations. The spacing between the volcanic lines or ridges is on the order of 15–20 km [10], corresponding to an elastic thickness of the lithosphere of 1–2 km in the model.

The rather straight and long lines of seamounts are indicative of a strong and coherent stress field near the ridge which overwhelms most perturbations. Tensile stresses in the ridge-perpendicular direction are expected near the axis as they constitute the force required for driving the passive upwelling of the mantle and for extending and fracturing of the lithosphere at the spreading center. It is also reasonable to expect a tensile stress maximum at some distance from the ridge axis. The ‘ridge-push’ force, contrary to its name, does not act on the accretionary plate boundary, but is distributed over the entire width of the plate [23]. If the thickness– $\sqrt{\text{age}}$  relation holds for the lithosphere and assuming perfect isostasy, then the force due to ‘ridge-push’ is constant over the plate and is probably mostly balanced locally by asthenospheric drag. The forces relevant near the ridge are then a plate-driving force due to slab-pull and resistive forces due to passive mantle upwelling, normal faulting near the ridge, and opening of the ridge itself. The force thus transmitted along the plate is lowest at the ridge and greatest (and constant) outward from the edge of the active ridge system and upwelling region. Stress is defined as force per cross-sectional area; since the plate thickness varies as  $\sqrt{\text{age}}$  away from the ridge, but is more nearly constant in the immediate vicinity of the ridge, a tensile stress maximum is expected at some distance from the ridge axis. Such a coherent stress field would not only explain the persistence of the volcanic lines and their relative invulnerability to minor perturbations, but it may also explain why the volcanic lines

terminate some 30 km from the ridge; closer to the ridge, the tensile stress becomes too weak to allow magma penetration through the lithosphere. Alternatively, the mechanism of magma transport toward the ridge axis may be more efficient near the axis, thus starving the near ridge environment of magma available for seamount formation.

As described in Section, Fig. 8 shows the model results after formation of 5 parallel chains of seamounts, but before further volcanism between the lines perturbs the regular pattern. Shen et al. [14] demonstrated that the individual lines of volcanoes compete with each other for melt. It is thus possible that the region between the volcanic lines has largely been drained of magma, thus allowing only the formation of small seamounts [10]. The suppression of late volcanism after formation of the volcanic lines is amplified by the fact that the late eruptions must, by definition, penetrate thicker and colder lithosphere.

The Rano Rahi volcanic field and its extension into the Puka Puka ridge system provide an ideal regime for application of our simple model because the area is well studied and the EPR is free of major perturbations there. The situation is more complicated at other parts of the EPR where transform faults, overlapping spreading centers and microplates, strongly alter the near-ridge stress field. While it is not clear if the major near-ridge volcanic edifices, such as the Easter chain, the Foundation seamounts, and the chain west of the Easter microplate are of hotspot (or hotline) origin or due to some other process, the morphology of these chains and their arrangement into sets of ridges [51] is likely controlled by the interaction of flexural stresses with the regional and local tectonic stress field.

## 5. Summary and conclusions

A simple model of volcano formation based on hydrofracture of the lithosphere in locations where magma pressure exceeds the local near-surface stress field can explain the formation of volcanic chains both on the South Pacific Superswell and near the southern EPR; the model complements the classical hotspot or plume models of

island chain formation in other locations. The chains are generally aligned with the direction of the most tensile principal tectonic stress. The propagation velocity of the volcanic chains depends on how much of a disturbance relative to the unperturbed state is required to cause an eruption, and how fast the individual volcanoes form.

The persistence and straightness of the near-ridge volcanic lines suggests that the tectonic stress field is coherent over great distances along the ridge axis and strongly deviatoric with the least compressive stress perpendicular to the axis. Such a stress field may be due to the force driving passive mantle upwelling near the spreading axis and is in agreement with observations of normal faulting near the ridge axis. While not well constrained observationally, the stress field on older parts of the Pacific plate may be similar in direction if the subduction zone to the north does not exert a significant stress, perhaps because of processes such as trench roll-back. Membrane stresses due to volcanic loads cause the volcanoes within near-ridge chains to coalesce into continuous ridges over time.

Local perturbations in the stress field due to transform faults, overlapping spreading centers, microplates, and propagators may result in volcanic patterns such as those observed in the Foundation seamount chain, the Easter chain, the volcanic ridges west of both the Easter microplate and the ancient Selkirk microplate, as well as possibly some of the volcanic ridges associated with transform faults (often termed 'leaky transforms').

If the stress field on older parts of the lithosphere is strongly deviatoric as well, island chains on the superswell may simply be a mid-plate analog of the near-ridge chains. However, for a weakly deviatoric stress field, the model predicts a pattern of volcanoes spreading radially outward; chains may then be formed if the sublithospheric melt is concentrated along hotlines which also correlate with observed medium wavelength geoid undulations. Our model based on lithospheric stresses is in agreement with the observation that volcanism is typically initiated at times

of plate motion reorganizations when the tectonic stress field changes. *[RV]*

## References

- [1] M.K. McNutt, K.M. Fischer, The South Pacific superswell. In: B.H. Keating, P. Fryer, R. Batiza, G.W. Boehlert (Eds.), *Seamounts, Islands, and Atolls*, Geophysical Monograph Vol. 43, AGU, Washington DC, 1987, pp. 25–34.
- [2] M.K. McNutt, Superswells, *Rev. Geophys.* 36 (1998) 211–244.
- [3] M.K. McNutt, L. Sichoix, A. Bonneville, Modal depths from shipboard bathymetry: there IS a South Pacific Superswell, *Geophys. Res. Lett.* 23 (1996) 3397–3400.
- [4] C.E. Nishimura, D.W. Forsyth, Anomalous Love-wave phase velocities in the Pacific: sequential pure-path and spherical harmonic inversion, *Geophys. J.R. Astron. Soc.* 81 (1985) 389–407.
- [5] K.G. Bemis, D.K. Smith, Production of small volcanoes in the Superswell region of the South Pacific, *Earth Planet. Sci. Lett.* 118 (1993) 251–262.
- [6] J.T. Wilson, A possible origin of the Hawaiian Islands, *Can. J. Phys.* 41 (1963) 863–868.
- [7] W.J. Morgan, Convection plumes in the lower mantle, *Nature* 230 (1971) 42–43.
- [8] P. Wessel, L. Kroenke, A geometric technique for relocating hotspots and refining absolute plate motions, *Nature* 387 (1997) 365–369.
- [9] D.S. Scheirer, K.C. Macdonald, D.W. Forsyth, S.P. Miller, D.J. Wright, M.-H. Cormier, C.M. Weiland, A map series of the southern East Pacific Rise and its flanks, 15°S to 19°S, *Mar. Geophys. Res.* 18 (1996) 1–12.
- [10] D.S. Scheirer, K.C. Macdonald, D.W. Forsyth, Y. Shen, Abundant seamounts of the Rano Rahi seamount field near the southern East Pacific Rise, 15°S to 19°S, *Mar. Geophys. Res.* 18 (1996) 13–52.
- [11] D.T. Sandwell, E.L. Winterer, J. Mammerickx, R.A. Duncan, M.A. Lynch, D.A. Levitt, C.L. Johnson, Evidence for diffuse extension of the Pacific plate from the Pukapuka ridges and crossgrain gravity lineations, *J. Geophys. Res.* 100 (1995) 15087–15099.
- [12] A. Barone, W.B.F. Ryan, Single plume model for asynchronous formation of the Lamont seamounts and adjacent East Pacific Rise terrain, *J. Geophys. Res.* 95 (1990) 10801–10827.
- [13] L. Fleitout, C. Moriceau, Short-wavelength geoid, bathymetry and the convective pattern beneath the Pacific Ocean, *Geophys. J. Int.* 110 (1992) 6–28.
- [14] Y. Shen, D.S. Scheirer, D.W. Forsyth, K.C. Macdonald, Trade-off in production between adjacent seamount chains near the East Pacific Rise, *Nature* 373 (1995) 140–143.
- [15] A. Cazenave, B. Parsons, P. Calcagno, Geoid lineations of

- 1000 km wavelength over the Central Pacific, *Geophys. Res. Lett.* 22 (1995) 97–100.
- [16] A. Yamaji, Periodic hotspot distribution and small-scale convection in the upper mantle, *Earth Planet. Sci. Lett.* 109 (1992) 107–116.
- [17] N. Baudry, L. Kroenke, Intermediate-wavelength (400–600 km), South Pacific geoidal undulations: their relationship to linear volcanic chains, *Earth Planet. Sci. Lett.* 102 (1991) 430–443.
- [18] W.F. Haxby, J.K. Weissel, Evidence for small-scale mantle convection from Seasat altimeter data, *J. Geophys. Res.* 91 (1986) 3507–3520.
- [19] F. Richter, Convection and large-scale circulation of the mantle, *J. Geophys. Res.* 78 (1973) 8735–8745.
- [20] Y. Shen, D.W. Forsyth, D.S. Scheirer, K.C. Macdonald, Two forms of volcanism: implications for mantle flow and off-axis crustal production on the west flank of the southern East Pacific Rise, *J. Geophys. Res.* 98 (1993) 17875–17889.
- [21] E.L. Winterer, D.T. Sandwell, Evidence from en-echelon cross-grain ridges for tensional cracks in the Pacific plate, *Nature* 329 (1987) 534–537.
- [22] A.M. Goodwillie, B. Parsons, Placing bounds on lithospheric deformation in the central Pacific Ocean, *Earth Planet. Sci. Lett.* 111 (1992) 123–139.
- [23] E.E. Davis, J.L. Karsten, On the cause of the asymmetric distribution of seamounts about the Juan de Fuca Ridge: ridge-crest migration over a heterogeneous asthenosphere, *Earth Planet. Sci. Lett.* 79 (1986) 385–396.
- [24] D.S. Wilson, Focused mantle upwelling beneath mid-ocean ridges: evidence from seamount formation and isostatic compensation of topography, *Earth Planet. Sci. Lett.* 113 (1987) 41–55.
- [25] R. Batiza, Abundances, distribution and sizes of volcanoes in the Pacific Ocean and implications for the origin of non-hotspot volcanoes, *Earth Planet. Sci. Lett.* 60 (1982) 195–206.
- [26] L.H. Kellogg, D.L. Turcotte, Mixing and the distribution of heterogeneities in a chaotically convecting mantle, *J. Geophys. Res.* 95 (1990) 421–432.
- [27] C.F. Hieronymus, D. Bercovici, Discrete alternating hotspot islands formed by interaction of magma transport and lithospheric flexure, *Nature* 397 (1999) 604–607.
- [28] M.K. McNutt, A.V. Judge, The superswell and mantle dynamics beneath the South Pacific, *Science* 248 (1990) 969–975.
- [29] J. Phipps Morgan, W.J. Morgan, Y.-S. Zhang, W.J.F. Smith, Observational hints for a plume-fed, suboceanic asthenosphere and its role in mantle convection, *J. Geophys. Res.* 100 (1995) 12753–12767.
- [30] R. Batiza, Y. Niu, W.C. Zayac, Chemistry of seamounts near the East Pacific Rise Implications for the geometry of subaxial mantle flow, *Geology* 18 (1990) 1122–1125.
- [31] M.L. Zoback, First- and second-order patterns of stress in the lithosphere: The World Stress Map project, *J. Geophys. Res.* 97 (1992) 11703–11728.
- [32] D.W. Forsyth, S. Uyeda, On the relative importance of the driving forces of plate motion, *Geophys. J.R. Astron. Soc.* 43 (1975) 163–200.
- [33] C. Lithgow-Bertelloni, M.A. Richards, The dynamics of Cenozoic and Mesozoic plate motions, *Rev. Geophys.* 36 (1998) 27–78.
- [34] D.M. Davis, S.C. Solomon, True polar wander and plate-driving forces, *J. Geophys. Res.* 90 (1985) 1837–1841.
- [35] C. DeMets, R.G. Gordon, D.F. Argus, S. Stein, Current plate motions, *Geophys. J. Int.* 101 (1990) 425–478.
- [36] S. Timoshenko, S. Woinowsky-Krieger, *Theory of Plates and Shells*, McGraw-Hill, New York, 1959.
- [37] D.L. Turcotte, G. Schubert, *Geodynamics: Applications of Continuum Physics to Geological Problems*, Wiley, New York, 1982.
- [38] A.M. Goodwillie, Short-wavelength gravity lineations and unusual flexure results at the Puka Puka volcanic ridge system, *Earth Planet. Sci. Lett.* 136 (1995) 297–314.
- [39] P. Wessel, A reexamination of the flexural deformation beneath the Hawaiian Islands, *J. Geophys. Res.* 98 (1993) 12177–12190.
- [40] D.L. Kohlstedt, B. Evans, S.J. Mackwell, Strength of the lithosphere: constraints imposed by laboratory experiments, *J. Geophys. Res.* 100 (1995) 17587–17602.
- [41] D.A. Clague, R.T. Holcomb, J.M. Sinton, R.S. Detrick, M.E. Torresan, Pliocene and Pleistocene alkalic flood basalts on the seafloor north of the Hawaiian Islands, *Earth Planet. Sci. Lett.* 98 (1990) 175–191.
- [42] C.F. Hieronymus, D. Bercovici, Hotspot volcanism: control on volcanic spacing and patterns, magma focusing, and discrete volcanoes vs. continuous ridges, *J. Geophys. Res.*, submitted for publication.
- [43] C. Canuto, M.Y. Hussaini, A. Quarteroni, T.A. Zhang, *Spectral Methods in Fluid Dynamics*, Springer, New York, 1988.
- [44] M.K. McNutt, D.W. Caress, J. Reynolds, K.A. Jordahl, R.A. Duncan, Failure of plume theory to explain mid-plume volcanism in the southern Austral Islands, *Nature* 389 (1997) 479–482.
- [45] A. Cox, D.C. Engebretson, Change in motion of the Pacific Plate at 5 Myr BP, *Nature* 313 (1985) 472–474.
- [46] R.G. Gordon, D.M. Jurdy, Cenozoic global plate motions, *J. Geophys. Res.* 91 (1986) 12389–12406.
- [47] M.K. McNutt, K. Fischer, S. Kruse, J.H. Natland, The origin of the Marquesas fracture zone ridge and its implication for the nature of hot spots, *Earth Planet. Sci. Lett.* 91 (1989) 381–393.
- [48] W.W. Sager, B.H. Keating, Paleomagnetism of the Line Islands seamounts; evidence for late Cretaceous and early Tertiary volcanism, *J. Geophys. Res.* 89 (1984) 11135–11151.
- [49] C. Lithgow-Bertelloni, M.A. Richards, Y. Ricard, R.J. O'Connell, Toroidal-poloidal partitioning of plate motions since 120 Ma, *Geophys. Res. Lett.* 20 (1993) 375–378.

- [50] J.M. O'Connor, P. Stoffers, J.R. Wijbrans, Migration rate of volcanism along the Foundation Chain, SE Pacific, *Earth Planet. Sci. Lett.* 164 (1998) 41–59.
- [51] N. Binard, P. Stoffers, R. Hekinian, R.C. Searle, Intra-plate en echelon volcanic ridges in the South Pacific west of the Easter Microplate, *Tectonophysics* 263 (1996) 23–37.
- [52] W.H.F. Smith, D.T. Sandwell, Predicted bathymetry: new global seafloor topography from satellite altimetry, *EOS* 77-46 (1996) 315.